Erciyes Üniversitesi
Fen Bilimleri Enstitüsü Dergisi
Cilt 41, Sayı 2, 2025

Erciyes University
Journal of Institue Of Science and Technology
Volume 41, Issue 2, 2025

Effect of ASTM-D638 Specimen Type on the Tensile Properties of Fused Deposition Modelling 3D-Printed PLA Specimens

Roaa GOMAA[1], Sara Saeed Abdulrahman ELTAHIR[2], Cağatay YILMAZ[1]*

[1] Department of Mechanical Engineering, Abdullah Gül University
[2] Department of Advanced Materials and Nanotechnology, Abdullah Gül University
*[1] Department of Mechanical Engineering, Abdullah Gül University

(Alınış / Received: 21.01.2025, Kabul / Accepted: 01.08.2025, Online Yayınlanma / Published Online: 30.08.2025)

Keywords
Fused Deposition Modeling (FDM), Polylactic Acid (PLA), Digital Image Correlation (DIC), Tensile Testing,

Abstract: This research examines how different ASTM-D638 specimen types affect the mechanical properties of 3D-printed PLA materials. Specimen types refer to specific configurations of test samples used in mechanical testing, as defined by ASTM-D638 standards, which include five different types: Type I – Type V. The standard outlines various specimen geometries and dimensions to ensure consistent and comparable testing procedures for polylactic acid-related studies. Computer-aided design models are created, and Fused Deposition Modeling 3D-printing is used to produce PLA specimens. Tensile testing and digital image correlation analysis are performed to measure the strength and strain of the samples, respectively. The study aims to provide comprehensive data on specimen type's impact on part properties and demonstrate a cost-effective strain measurement method using DIC and a smartphone. The methodology includes computer-aided design modeling, 3D-printing, surface preparation, tensile testing, DIC analysis using Ncorr, and MATLAB data processing. Results show stress-strain curves and average strain values, with Type I and Type II exhibiting the highest ultimate tensile strength of 43.179 MPa and 43.164 MPa, respectively. However, Type V is the most optimum option due to its short printing time and low filament usage, which are 5 times less than Type I, and a reasonable strength of 42.640 MPa. This research fills a knowledge gap on specimen design's influence on 3D-printed part properties, providing valuable insights for future research.

ASTM-D638 Numune Tipinin Erimiş Biriktirme Modelleme 3D Baskılı PLA Numunelerinin Çekme Özelliklerine Etkisi

Anahtar Kelimeler
Eriyik Yığma Modellemesi, Poli Laktik Asit (PLA), Sayısal Görüntü Korelasyonu, Çekme Testi,

Öz: Bu araştırma, farklı ASTM-D638 numune türlerinin 3D-baskılı PLA malzemelerinin mekanik özelliklerini nasıl etkilediğini incelemektedir. Numune türleri, ASTM-D638 standartlarında tanımlandığı gibi, beş farklı türü içeren, mekanik testlerde kullanılan test numunelerinin belirli konfigürasyonlarını ifade eder: Tip I – Tip V. Bu standart, tutarlı ve karşılaştırılabilir test prosedürlerini sağlamak için çeşitli numune geometrilerini ve boyutlarını özetlemektedir. Standart, Polilaktik asitle ilgili çalışmalar için tutarlı ve karşılaştırılabilir test prosedürleri sağlamak amacıyla çeşitli numune geometrilerini ve boyutlarını özetlemektedir. Bilgisayar destekli tasarım modelleri oluşturulur ve PLA numuneleri üretmek için Erimiş Biriktirme Modelleme 3D-baskı kullanılır. Numunelerin mukavemetini ve gerinimini ölçmek için sırasıyla çekme testi ve Dijital Görüntü Korelasyonu analizi yapılır. Çalışma, numune türünün parça özellikleri üzerindeki

etkisine ilişkin kapsamlı veriler sağlamayı ve DIC ve akıllı telefon kullanılarak uygun maliyetli bir gerinim ölçüm yöntemi göstermeyi amaçlıyor. Metodoloji, CAD modellemeyi, 3D yazdırmayı, yüzey hazırlığını, çekme testini, Ncorr kullanılarak DIC analizini ve MATLAB veri işlemeyi içerir. Sonuçlar, Tip I ve Tip II'nin sırasıyla 43,179 MPa ve 43,164 MPa ile en yüksek nihai gerilme mukavemetini sergilediği gerilim-gerinim eğrilerini ve ortalama gerinim değerlerini gösterir. Ancak Tip V, kısa baskı süresi ve Tip I'e göre 5 kat daha az olan düşük filament kullanımı ve 42.640 MPa'lık makul mukavemeti nedeniyle en optimum seçenektir. Bu araştırma, numune tasarımının 3D baskılı parça özellikleri üzerindeki etkisine ilişkin bilgi boşluğunu doldurarak gelecekteki araştırmalar için değerli bilgiler sağlıyor.

*İlgili Yazar, email: yilmaz.cagatay@agu.edu.tr

3D-printing is one of the most developing technologies in the realm of additive manufacturing (AM). Commonly used in the production of molds and prototypes [1] 3D-printing allows the fast production of customizable lightweight intricate objects of a wide range of sizes, styles, and materials, that are hardly replicable using other manufacturing methods [2,3]. Fused deposition modelling (FDM), also known as fused filament fabrication (FFF), is one of the leading 3D-printing techniques in the production of plastic materials [4]. It represents an additive manufacturing technology that facilitates the creation of three-dimensional models via a CAM process [5]. The printing process relies on the controlled extrusion of material through a specialized heated nozzle [6] at a temperature typically less than 250˚C [7].

There are different types of polymer filaments used in FDM. Acrylonitrile butadiene styrene (ABS) and polylactic acid (PLA) are primarily used in FDM printers due to their suitable melting temperatures that allow nozzle excursion while retaining shape [8]. However, PLA filament, which is made of biodegradable thermoplastic material with a printing temperature ranging from 190 - 230˚C, ensures high performance and acceptable mechanical properties post-printing [9]. FDM technology is well-regarded for its user-friendliness, cost-efficiency, lightweight, and high strength-to-weight ratio characteristics [10], which makes it a valuable tool for development, prototyping, and manufacturing. Consequently, it is crucial to emphasize the significance of understanding the effect of the 3D-printing parameters and adjusting them to achieve the optimal required mechanical properties of a 3D-printed part.

The FDM process outcomes and efficiency of the produced parts are influenced by a range of printing parameters. Therefore, a comprehensive examination of these printing parameters is essential to reach the required properties for a 3D-printed part. This is emphasized in the literature, Popescu et al. [11] a literature review to investigate the key FDM variables, including printing process parameter selection and filament material, that affect the mechanical properties of FDM printed parts across various polymer types, including PLA. The results revealed that the tensile characteristics of FDM parts are mainly influenced by the orientation of the printed layers, the thickness of each layer, the density of the internal infill structure, and the orientation in which the object is built. However, the effects vary depending on the printer and polymer employed. This literature perception is consistent with the current study approach; however, while citing ASTM D638 as a typical standard for tensile testing, the researcher makes no differentiation between the many specimen types specified in the standard.

Kamaal et al. [12] explored the most efficient combination of printing parameters needed for producing 3D-printed parts with high tensile strength while minimizing material usage. They used specimen models that corresponded to the ASTM D638 standards. They examined variables such as the building direction, infill percentage, and layer height, as these factors were identified as having a significant impact on the printed parts' mechanical performance. According to their findings, the investigation results indicate that the specimen, which had an 80% infill rate, was constructed in the X direction, and had a layer height of 0.2 mm, exhibited the highest tensile strength.

Similarly, in a study conducted by Kam et al. [13], an examination was carried out to explore how various process parameters within the FDM manufacturing technique influence different mechanical properties, including the tensile strength, of 3D-printed Polyamide12 samples. The research revealed that among the parameters studied, the most significant impact on tensile strength was attributed to layer thickness and occupancy rate. The study identifies the optimal parameter values for achieving the highest tensile strength. These values were determined to be a layer thickness of 0.25 mm, an occupancy rate of 50%, a filling structure set to rectilinear, and an extruder temperature of 250°C. Therefore, these findings were taken into consideration when selecting the printing parameters for the current study.

Qattawi et al. [14] conducted an empirical investigation aiming to determine the individual impact of various FDM processing parameters on both mechanical attributes and the repeatability of dimensional accuracy of PLA parts. The study particularly investigated the influence of building orientations, infill percentage, infill pattern, print speed, extrusion temperature, and layer height on the mechanical properties of the printed samples. To investigate these mechanical properties, the researchers employed a tensile testing method following ASTM-D638 type IV standards for plastic tensile testing. The findings of this research revealed that higher infill percentage and higher layer height have a positive effect on the mechanical properties of printed parts. The application of a layer height of 0.25 mm was found to result in a small dimensional error in thickness, which reflects an improved print accuracy. Moreover, as the extrusion temperature increased, there was an evident improvement in the mechanical properties, which is attributed to the improved cohesion within the extruded layers and between successive layers. Conversely, it was observed that print speed and infill patterns had a relatively minor impact. Hence, in the current study, to optimize the mechanical properties of the printed specimens, a combination of higher extrusion temperatures, larger layer heights, and building orientations aligning the layers with the load direction in the same plane is utilized.

The printing parameters of the FDM technique decide the time and the polymer material consumption needed for printing a part. Therefore, to provide a thorough study of this technique, the factors of time and material should be considered in the literature. For instance, Ćwikła et al. [7] investigated the specific mechanical strength characteristics demonstrated by standardized specimens printed using cost-effective materials, ABS, and a budget-friendly 3D-printer. They assessed the impact of various printing variables, including infill pattern and infill density. The results indicated that, in order to produce a lightweight component with high strength, the optimal parameters recommended the adoption of a honeycomb infill pattern, with a fill density between 40-50%. This finding highlighted that samples printed with less than 100% infill could attain comparable strength to solid counterparts, all while conserving time and materials. However, it's worth noting that choosing another infill pattern could accelerate the printing process, but at the cost of structural strength.
It can be noticed when assessing the mechanical properties of 3D-printed parts that the ASTM D638 standard test method plays a pivotal role. The ASTM D638 standard, which is specified by the American Society for Testing and Materials as the standard test procedure to find the tensile properties of plastics, is widely used. This test method is used for testing the tensile properties of plastic materials with specifications on how to evaluate mechanical properties such as strength, stiffness, and ductility. Additionally, ASTM D638 also defines specimen types, Types I to V, which are used to accommodate different materials and testing requirements through varying shapes, sizes, and geometries. For general-purpose testing of rigid or semi-rigid polymers with a thickness of less than 7 mm, Type I specimens are recommended for use. For materials that break outside of Type I's limited range, Type II is recommended. Thick specimens that are between 7 and 14 mm in thickness are classified as Type III. Type V works effectively when there is a relatively small amount of material available or when high-throughput testing in narrow spaces is required, whereas Type IV is commonly used for direct comparison between rigid and non-rigid materials. Therefore, it is necessary to examine the ASTM D638 standard for PLA material within the additive manufacturing context.

For example, Jatti et al. [15] examined the influence of multiple FDM 3D printing parameters, such as extrusion temperature, print speed, layer height, and infill density, on the tensile strength of PLA material. The tensile test was performed with Type V specimen geometry according to the ASTM D638 standard. The findings confirmed that a medium extrusion temperature, a medium printing rate, an increased infill percentage, and a lower layer height all combined to maximize tensile strength. Using 100% infill with a low layer height of 0.087 mm, optimization results demonstrated better interlayer adhesion, producing a material with a maximum tensile strength of 55.475 N/mm2.

A similar study, Syaefudin et al. [16] particularly examined how the printing orientation parameter affects the tensile strength of 3D-printed PLA and ABS parts. The study investigated the effects of three printing orientations (0°, 45°, and 90°) using the ASTM D638 Type IV specimen design type, with a layer thickness of 0.1 mm. They examined the mechanical properties, tensile strength, yield strength, and elastic modulus. The findings demonstrated that printing orientation has a significant impact on tensile strength. The highest ultimate tensile strength (UTS) of the PLA specimens printed at 0° was 35.16 MPa, whereas the UTS of the specimens printed at 90° decreased by 52.8%. This emphasizes how important printing orientation is in determining the mechanical behavior of FDM-printed PLA pieces.

Letcher and Waytashek [17] similarly researched the effects of raster orientation on mechanical parameters, including tensile strength, in PLA specimens that were 3D printed using an entry-level FDM printer. With a 100% infill pattern, three raster orientations (0°, 45°, and 90°) were implemented. They also utilized the ASTM D638 Test Methods for Tensile Properties of Plastics of a Type I specimen type with dimensional deviations. The results

demonstrated that the greatest UTS of 64.03 MPa was observed in PLA specimens manufactured at a 45° raster angle, followed by a UTS of approximately 58 MPa at 0° raster orientation and 54.01 MPa at 90°.

Adding to the usage of ASTM D638 specimen types, Yeole [18] delivered an important contribution by utilizing the ASTM D638 Type IV standard in their tensile testing and analysis of 3D-printed PLA specimens. The authors indicate that the majority of the previous investigations mainly employed ASTM D638 Type I specimens in the tensile strength analysis of PLA materials. 100% infill, 0.3 mm layer height, and 230°C extruder temperature were used to print the Type IV specimens. The investigation revealed that Type IV specimens can adequately represent PLA performance under tensile loading conditions, with a maximum UTS of 54.46 MPa.

Expanding upon the assessment of mechanical properties in 3D-printing, the Digital Image Correlation (DIC) technique is integrated into the current study to examine the mechanical behavior of 3D-printed components. DIC is a free, open-source tool that can be seamlessly incorporated with MATLAB using the Ncorr analysis code, making it accessible to researchers. Additionally, the setup for DIC can process data obtained even from smartphone cameras, enhancing accessibility and reducing the need for specialized equipment. This addition will not only aid in the current study but also pave the way for future researchers to conduct their studies economically and with minimal tools.

DIC techniques work by real-time analyzing digital images of a test object captured at various stages of deformation [19]. DIC stands as a non-contact optical method with the remarkable capacity to carry out a comparison of the grey intensity changes in images taken before and after deformation [20]. The numerical system calculates surface displacement by tracking pixel units and constructing comprehensive two-dimensional vector fields of deformation and strain variations. DIC is utilized in numerous applications. The most prevalent utilization is within the domain of fracture mechanics, including plastic deformation and the investigation of fracture surfaces in specimens undergoing tensile loading. DIC can be credited to Peters et al. [21], marking a pioneering advancement in the field of experimental stress analysis.

DIC is a resourceful technique that correlates various patterns like grids, dots, lines, and random patterns. In practice, a random speckle pattern is usually utilized [20]. The effectiveness and accuracy of DIC depend on several factors, encompassing both the quality of image acquisition and the computational analysis of the data. For instance, Wang et al. [22] evaluated measurement uncertainties in their DIC experiments by studying their imaging system. Their research suggested the multiple-image approach to enhance the DIC measurement precision by taking a minimum of 15 images over a specified time frame to average deformation. This reduces the uncertainty values in displacement parameters, ranging from 0.06 to 0.14 pixels, and displacement gradients, ranging from 0.0039 to 0.0085.

Another predominant factor is the quality of the speckle pattern on the specimen. Research by Lecompte et al. [23] showed that the size of the speckles and their density play a crucial role in this regard. Crammond et al. [24] also investigated the impact of speckle size and density on deformation measurements using DIC. They found that a scarce speckle pattern resulted in higher errors when using high-magnification imaging. Introducing finer speckles with an airbrush effectively reduced measurement errors, especially as the subset speckle density increased. Moreover, it is suggested to use larger speckles, as they provide more distinct shape features.

The size of chosen subsets significantly influences measurement accuracy. As shown by Yaofeng et al. [25] using larger subsets results in reduced standard deviations and improved accuracy. However, the optimal subset size depends on the quality of the speckle pattern. For instance, intricate speckle patterns may necessitate larger subsets to capture distinctive features, while high-contrast speckle patterns can yield precise results with smaller subsets. Likewise, Berfield et al. [26] utilized DIC for comprehensive micro- and nanoscale strain measurement. Their research emphasized the correlation precision, influenced by speckle pattern quality and camera resolution. They also highlighted the emphasis on subsection dimensions in correlation analysis.

DIC techniques employ computational algorithms to achieve sub-pixel precision, facilitating high-resolution data extraction and surface deformation measurement from digital images. According to Pan et al. [27], DIC fundamentally involves matching identical subsets in both the reference and deformed images to derive full-field displacements. Various correlation functions are employed to evaluate the similarity between the reference and deformed images, and this is accomplished through the highly accurate Newton–Raphson (NR) algorithm. NR is prominent for its outstanding sub-pixel displacement tracking accuracy, regardless of relative deformation and rotation of the deformed subset, making it the ultimate choice for achieving the highest sub-pixel registration accuracy and widespread applicability.

Ncorr is a modern open-source DIC software. It is a subset-based 2D DIC tool that utilizes advanced DIC algorithms, primarily relying on the NR algorithm for deformation computation [28]. It is developed within the widely used MATLAB platform. Ncorr's main goal is to provide well-documented and adaptable code, allowing users to customize it extensively to meet their specific needs. The core operation of Ncorr's algorithms involves subset deformation, where subsets are initially circular groups of points strategically placed at integer pixel coordinates in the reference image. The transformation of these points' coordinates from the reference image to the current arrangement follows a constrained linear transformation at a first-order level.

Ali et al. [29] conducted an empirical investigation assessing the effectiveness of the DIC technique in measuring strain deformations. This research endeavor closely adhered to the guidelines laid out, encompassing recommended instructions for image obtaining, information extraction, image processing, and strain calculation. This paper serves as an exhaustive and methodically structured demonstration of the procedural details and methodologies of DIC. Particularly, the study investigates the application of the Ncorr open-source platform for the implementation of DIC, offering a thorough exploration of the technique.

Previous studies have examined the impact of FDM process parameters on tensile characteristics [7,12–14]. However, there is a lack of research on the impact of 3D-printed specimens designed based on the ASTM-D638 types and their effect on the tensile mechanical properties of PLA 3D-printed parts. Instead, it is observed that the specimen types are interchangeably used without clear justification or instruction on the most suitable design for PLA 3D-printed specimens' applications. According to the in-depth literature review focusing on FDM, 3D-printing, and DIC, there is still a lack of targeted research on the influence of the ASTM D638 specimen type on the tensile mechanical characteristics of PLA. This study builds on previous research by systematically testing each of the five ASTM D638 specimen types under consistent scenarios using tensile testing and DIC analysis. Therefore, assessing how the designs of the five types of ASTM-D638 impact not only mechanical performance but also production efficiency in terms of print time and material usage is where the novelty of this study lies. This presents a comprehensive analysis of the optimum specimen type for PLA in terms of tensile characteristics, manufacturing duration, and cost-effectiveness. This is achieved by utilizing DIC analysis to obtain the bi-axial strain observed during tensile testing by using a simplified phone camera-based setup and the open-source Ncorr platform for data processing.

2. Materials and Methods

This study utilizes an experimental approach as its methodology. The initial step involves the creation of CAD models for the design of the specimens. Subsequently, the specimens were 3D-printed, and preparatory measures were taken before conducting the tensile test, including surface preparation. The actual tensile test is then performed. To analyze the test results, the DIC method is employed, utilizing the open-platform Ncorr application, and the data obtained from Ncorr is further processed and refined. MATLAB is utilized to calculate the UTS of all the specimen types based on the refined data acquired from the analysis.

2.1. Specimen Design

The specimen types and their dimensions were selected in accordance with the ASTM-D638 standard, as illustrated in Table 1. The ASTM D638 standard was chosen over other established standards (e.g., ISO 527-2) since it includes a more varied standardized geometry of the specimens. It covers five specimen types (Types I–V), which are in accordance with the objectives of this study, to assess how different test sample configurations affect the mechanical properties of PLA materials that are 3D printed when subjected to mechanical testing. In addition, ASTM D638 is consistent with standardized strain measuring techniques, such as the crosshead displacement and DIC, making it an effective choice for this study, as it includes camera-based non-contact testing. It is also very relevant to this study due to its already established application in the literature research on 3D-printed polymer components [12].

To create 3D models of the five specimen types described in the standard paper, SOLIDWORKS software was employed. The SOLIDWORKS models, which accurately reflected the standard dimensions, can be observed in Figure 1. In order to prepare the models for the 3D-printing process, the file format of all the 3D models was converted to Stereolithography (.STL) files, which are compatible with the Raise 3D-printer.

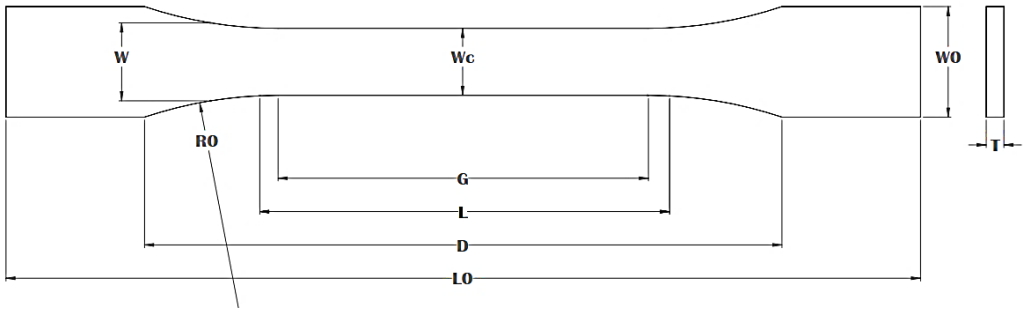

(a) Type I, II, III, and V

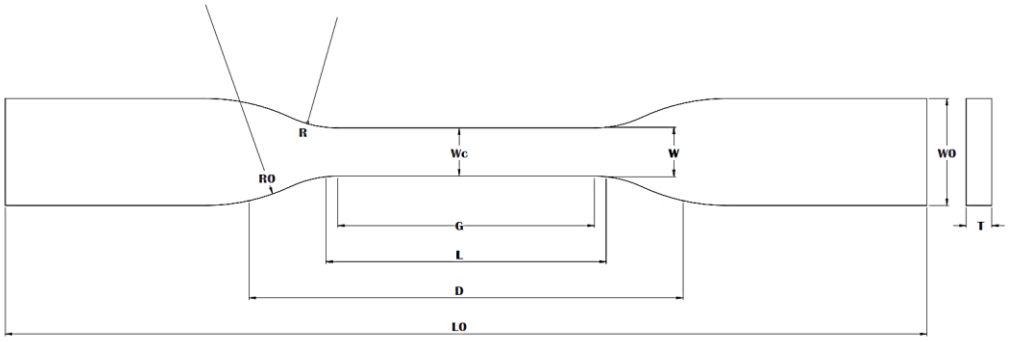

(b) Type IV

Figure 1. 2D Designs of samples, a) Type I, II, III, and V, b) Type IV

Table 1. Specimen Dimensions, mm

Dimensions	***T-Thickness of 3.2***					
	Type I	Type II	Type III	Type IV	Type V	Tolerances
W-Width of narrow section	13	6	19	6	3.18	±0.5
L-Length of narrow section	57	57	57	33	9.53	±0.5
WO-Width overall	19	19	29	19	9.53	+6.4 / +3.18 (Type V)
LO-Length overall	165	183	246	115	63.5	-
G-Gage length	50	50	50	25	7.62	±0.25/ ±0.13 (Type IV)
D-Distance between grips	115	135	115	65	25.4	±5
R-Radius of fillet	76	76	76	14	12.7	±1
RO-Outer radius (Type IV)	-	-	-	25	-	±1

2.2. 3D-Printing

The printing stage started by extensively reviewing the literature on printing parameters to select the most optimal settings and parameters for this study's needs. For instance, the optimal printing temperature was found to be in the range 190 - 230˚C [9] and 250°C [13,18]. The infill density was 100% [15,17,18]. In the current study, the nozzle deposited material back and forth along the length (x direction), which matches the 0° raster angle or infill angle [12,16,17]. However, when attempting to apply the literature-based data, unforeseen issues arose during the initial printing procedures. These included an inadequate heatbed temperature with respect to the room temperature, resulting in the detachment of parts from the printing bed. Additionally, unexplained G-code errors, such as the appearance of diagonal solid lines across the parts, complicated the process. These challenges were visually observed during the trial printing process.

Consequently, a trial-and-error approach was utilized, involving minor adjustments to the printing parameter values obtained from the literature. The objective of the adjustments was to discover the optimal parameters that would meet the geometric requirements for all ASTM-D638 specimen types without compromising the strength properties of the parts. This iterative process allowed for the identification of printing parameters that resolved the initial issues and ensured the successful printing of the desired specimens. The selected printing parameters can be seen in Table 2 [30] and they were kept constant during the production of all the specimens.

The used PLA+ filament model was a red eSUN brand. Its mechanical properties include a tensile strength of 60 MPa and a flexural modulus of 1973 MPa, according to the supplier's datasheet [31] illustrated in Table 3. The filament spool was stored in a dry environment at room temperature prior to printing to avoid any moisture-related defects. Also, the 3D-printing process was conducted in dry conditions to prevent bubbling or poor layer adhesion.

Table 2. 3D-Printing Parameters

3D-Printing Parameter	***Values***
Filament Type	PLA
Layer thickness (mm)	0.25
Infill density (%)	100
Infill angle	0
Filling structures	Solid lines
Filament extruder temperature (°C)	215
Heatbed temperature (°C)	80
Nozzle diameter (mm)	0.4
Number of Extruder nozzle	1
Extruder width (mm)	0.38
First layer speed (m/s)	8
Speed (m/s)	30
Retraction Speed (m/s)	20
Shell numbers	1
Processor	ideaMaker
Platform addition – Brim numbers	10

Table 3. PLA Filament Properties [31].

Filament Properties	***Values***
Filament Type	PLA
Brand	eSun
Model	PLA+
Weight (Kg)	1 Kg/Spool
Color	Red
Filament Diameter (mm)	1.75 ±0.05
Filament Length (m)	340-345
Printing Temperature (°C)	210-230
Density (g/cm³)	1.23
Tensile Strength (MPa)	60
Bending Strength (MPa)	74
Flexural Modulus (MPa)	1973
IZOD Impact Strength (kJ/m2)	6

A total of 31 specimens were produced in this study, with six specimens printed for each type except for Type III, which had seven specimens. The pictures of the printed specimens are shown in Figure 2. The printing parameters were set according to the specifications above. The printing infill was fully dense (100%) using a grid solid lines pattern and a single outer shell. This means the inside was filled with PLA filament, but the outer contour consisted of a single printed perimeter wall. This was done to produce uniform internal density in all the samples while minimizing printing time and

material use at the outer surfaces. In order to align the layers perpendicular to the tensile tension, all specimens were printed flat on the printing plate (angle = 0). The layer height of 0.25 mm was chosen based on the optimal layer height found in the literature. Particularly, the studies [13,14] showed optimal printing accuracy by adopting 0.25 mm as layer thickness. Also, [13] particularly adopted solid infill for consistent mechanical performance.

The specimen designs were accepted when they agreed with the standardized measurements specified by ASTM-D638 types. Therefore, to ensure quality control, the dimensions of the printed specimens were carefully inspected using a caliper instrument to ensure they met the standard dimensions. Additionally, a successful print was characterized by minimal to no defects and a smooth surface on the specimen. It was observed that all the printed specimens fulfilled these criteria. Furthermore, the average thickness and width values of each type were recorded as reference values for subsequent calculations and analysis.

(a) Type I Specimen

(b) Type II Specimen

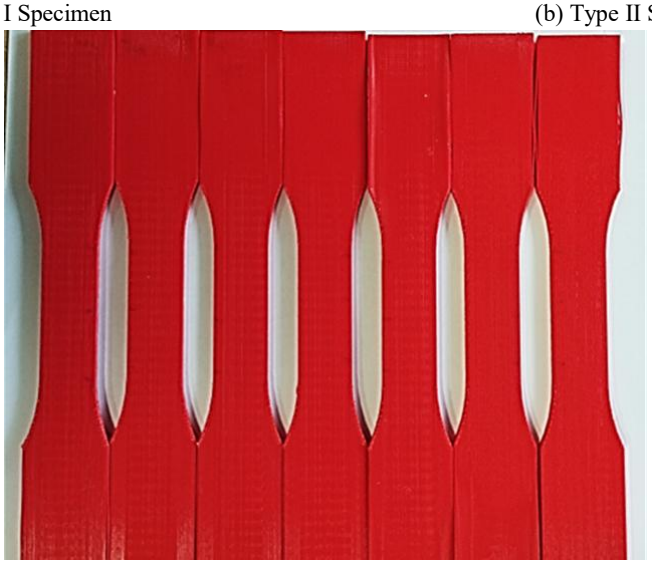

(c) Type III Specimen

(d) Type IV Specimen

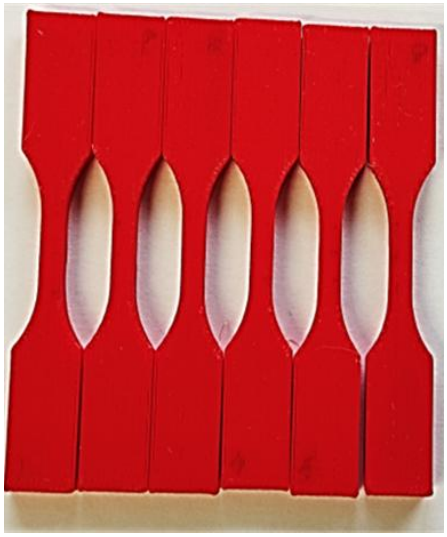

(e) Type V Specimen

Figure 2. Printed specimens

2.3. Surface Preparation

To conduct the DIC analysis during the tensile testing of the specimens, a surface preparation procedure was carried out. The surface of each specimen underwent a coating process using opaque white spray paint. Multiple layers, typically 2–3, were applied until the entire surface was uniformly covered and leveled with white paint. This coating process is necessary to cover the initial filament color, level any bumps caused during 3D printing, and provide a white background for DIC analysis. To meet the requirement of DIC parameters, which necessitate an adequate number of speckles, a pattern consisting of black speckles was manually applied onto the white-coated surface. This was done carefully to ensure that all the specimens were adequately covered with the black speckle pattern Figure 3.

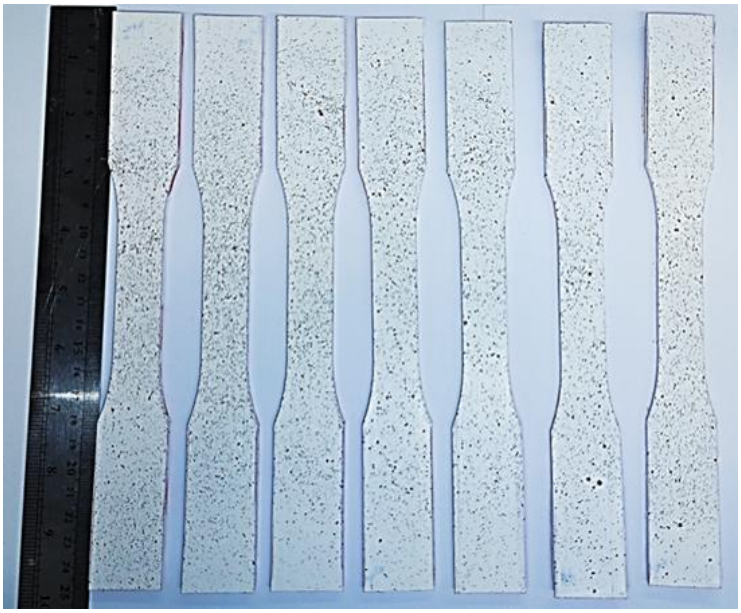

Figure 3. Surface Finish of Type III Specimens

2.4. Tensile Testing

The setup for the DIC system involved placing a high-resolution smartphone camera on a stable tripod at an appropriate distance from the specimen being tested. The camera specification includes a 26mm, f/1.8 lens with 50-megapixel resolution and 1080 Pixels at 30 frames per second. The distance was carefully determined to ensure that the recordings would maintain excellent quality and resolution. Furthermore, it was essential to maintain a consistent distance for all types of samples to ensure that the recording parameters remained constant. Another important consideration in setting up the DIC system was ensuring sufficient brightness during the recording process. To meet this requirement, two flashlights were positioned on tripods, focused on the testing specimens at the same distance as the smartphone camera, ensuring that the appropriate brightness level was achieved for

the recording of the test. The recording duration of the testing was carefully synchronized to begin precisely when the tensile testing machine initiated its operation and ended at the moment of fracture occurrence.

A Shimadzu AGS-X Universal Testing Machine was used to conduct tensile tests with non-shift wedge-type grips on all printed specimens. To maintain consistency and minimize the influence of testing parameters on the material's behavior and mechanical properties, the machine was operated with constant settings. The crosshead speed of the machine remained steady at a rate of 5 mm/minute throughout the testing process.

The gauge length, which is the effective length of the specimen used for measuring strain and elongation, was determined based on the information provided in ASTM-D638 for each sample type. Careful attention was given to ensure that the gauge length was set accurately in accordance with the ASTM-D638 standard for all specimens, except for type three. Due to limitations in the maximum distance of the grips, the gauge length for all type three specimens was adjusted to 10 mm more than the standard value, the lowest modification that could be applied. However, the implications of this adjustment could lead to a slight reduction in the measured stress values of the tensile testing caused by the misalignment and the extended deformation zone. Moreover, the wider region introduced by the adjusted gauge section increases the chance of strain localization and stress concentration, especially around the transition zones between the gauge and grip sections. To prevent such challenges in further research, potential mechanical adjustments, such as providing detachable grips of multiple geometries and sizes that accommodate larger testing specimens, can be implemented to ensure methodological rigor and alignment with industry standards. It should be noticed that this adjustment was considered when calculating engineering stress and strain.

To prevent premature fracture, the applied forces on the specimens gradually increased during the testing procedure. Additionally, great care was taken during the installation of the specimens and adjustment of the machine's grips to ensure proper alignment and installation for all 31 specimens. These measures were implemented to ensure reliable and precise results by maintaining constant parameters throughout the testing process.

2.5. DIC – Ncorr Analysis

The DIC method, utilizing the open-platform Ncorr application, was employed to analyze the recorded data of the tested specimens. The first step of the DIC analysis involved converting the recording videos into a series of images. This conversion was carried out using an appropriate software program capable of extracting images from videos. The recording of each tested specimen was captured and processed to extract a set of images at a rate of one image per second. Consequently, the total number of images obtained for DIC analysis varied depending on the duration of the testing recordings. For Type I, the range of images analyzed was between 57 and 68, while Type II had 43 to 52 images. Type III included 62 to 70 images, Type IV consisted of 29 to 33 images, and finally, Type V had the lowest number of images, ranging from 20 to 25.

The MATLAB software was utilized to perform the DIC analysis on the acquired images. The Ncorr program was executed by entering the command "handles_ncorr = ncorr". This led to the compilation of the files and the appearance of the Ncorr program menu, which allowed for the arrangement of the images and DIC parameters. The DIC analysis process required the first image to serve as a reference image, representing the initial state without any loading or deformation. Subsequent images were then uploaded and compared to the reference image for analysis. The DIC parameters began with the definition of a region of interest (ROI) that included only the boundary around the tested specimen, where deformation or fracture was expected to occur.

Several parameters could be adjusted to facilitate the strain computation process. The key parameters in this study were the subset radius, subset spacing, number of threads, and seeds. The values assigned to these parameters were determined based on the work of Ali et al. [25] and a trial-and-error approach until optimal values suitable for all specimens were identified. The placement and number of seeds provided initial estimates for the DIC analysis. Before initiating the actual analysis, the seeds were verified to ensure the accuracy of the process by confirming that speckle movement was detectable and that the number of frames was sufficient to capture it effectively. In this study, a subset radius of 23 units was selected as the smallest radius that effectively eliminated noisy strain data. The spacing between subsets was set at 2 units, while the thread and seed numbers were both

set to 1. Figure 4 illustrates the selected DIC parameters, including subset radius and spacing, as configured in the analysis software. It is essential to note that a single seed and thread could impact the robustness of the correlation in areas with complex or highly localized strain; however, this was not a concern for the study's relatively uniform strain distributions. This method was utilized to reduce computational load, but future research might examine the usage of multiple seeds or enhanced thread processing in highly strained regions.

Following the displacement analysis, a calibration and scaling procedure was performed. This step involved converting the pixel values to a unit of measurement, which was millimeters, to obtain measurable displacement values. Finally, the strain computation yielded values for the Exx (transverse strain) and Eyy (longitudinal strain) planes. Figure 5 illustrates how the contour of strain can provide a visual representation of the strain value associated with the applied load. The resulting data were saved as a MATLAB Data (.mat) file, allowing for further analysis and processing of the data.

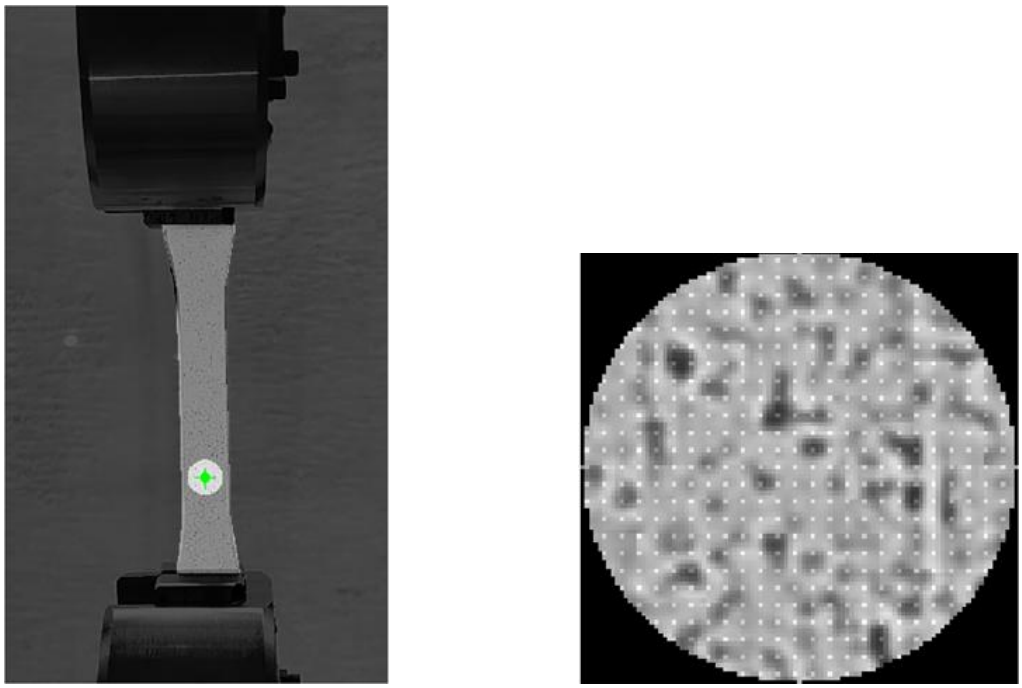

(a) Subset Location (b) Subset

Figure 4. DIC Set up parameters

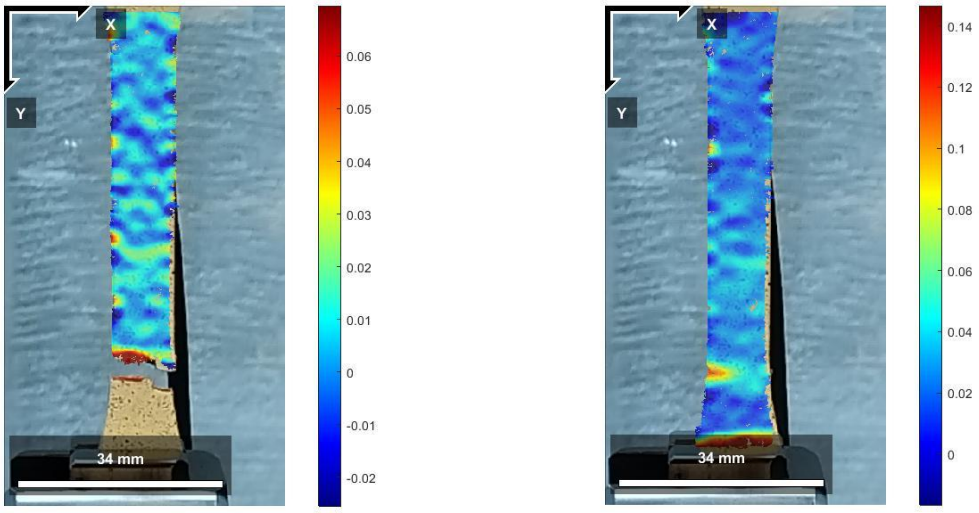

(a) After Breaking (b) Before Breaking

Figure 5. Ncorr Results Example

The data obtained from the Ncorr displacement analysis was processed using MATLAB software. The code imports all the required data, including data from the tensile machine and Ncorr data. The data from the tensile machine consists of force and stroke measurements over time. It is utilized to determine the stress on the specimen by dividing the force by the cross-sectional area of the specimen, which is calculated based on the dimensions provided in Table 1. The maximum stress is computed to obtain the average UTS.

The strain values obtained from the Ncorr displacement data analysis necessitate processing. Non-zero strain values from each frame are filtered, and unnecessary zero values originating from the background or unmoving parts in the tensile test are removed. Using the filtered data, the average strain (Exx and Eyy) for each frame is calculated. Since the obtained data is dependent on the number of frames, which is significantly lower than the stress data points, the strain values are interpolated. This allows for the display of the stress-strain curve on the same graph.

3. Results

The MATLAB code provided a set of three graphs displaying the behavior of the stress-strain curve of Exx, the change in length of the specimen in the direction of the applied force, the stress-strain curve of Eyy, the change in width of the specimen perpendicular to the direction of the applied force, and the average strain curve of Exx and Eyy against the frame. Fitted curves are generated using MATLAB's fit function with a first-degree polynomial model to capture the general trend of stress-strain data points. R^2 values were reported to evaluate the reliability of the fitting, where $R^2 > 0.9$ indicates low noise and a reliable fit, while $R^2 < 0.7$ suggests significant noise or disturbances in the data. Since this research is conducted on a sample of 30 specimens of 5 different ASTM-D638 types, many chart results that resemble one another were obtained from each type. Therefore, the chart results of one specimen of each type are discussed in this paper.

The results of Type I are depicted in Figure 6. Figure 6 (a) exhibits a declining trend, indicating a reduction in specimen width as tensile force is exerted. Conversely, Figure 6 (b) displays an upward trend, indicating elongation as tensile force is applied. The average strain values for Exx and Eyy are also presented in Figure 6(c). Notably, the Eyy strain exhibits an increasing slope until the point of fracture, whereas the Exx strain decreases.

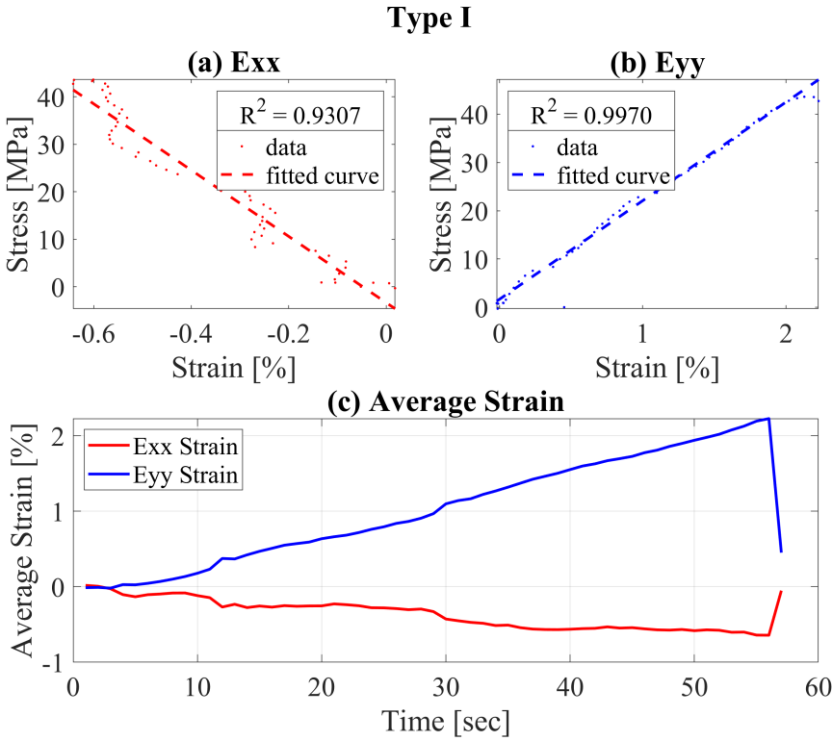

Figure 6. Type I Results

The results of Type II are illustrated in Figure 7. The stress-strain curve for Exx, the stress-strain curve for Eyy, and the average strain curve for Exx and Eyy exhibit similar patterns to those observed in Type I results. However, in Figure 7(a) and (b), notable irregularities are observed in the data points, which appear scattered and noisy. Additionally, the R^2 value of Figure 7 (a) is 0.7359, indicating noise in the fit plotting. Similarly, in Figure 7 (c), the average values of Exx and Eyy display spiky behavior. These irregularities may be attributed to challenges encountered in detecting the speckle patterns during the Ncorr displacement analysis. Notably, Type II specimens possess the lowest width-to-length ratio, implying a relatively longer and thinner structure. Consequently, the presence of fewer speckle patterns within the gauge length area and difficulties in capturing speckle movement with a smartphone camera could contribute to these issues, which may affect the accuracy of the measurements and interpretation of the material's mechanical properties. These problems can be addressed by recognizing that the size of the speckles significantly impacts the precision of displacement measurement through the DIC method. Therefore, it is realized that to ensure precise measurements, speckle patterns must maintain a size ranging from 2 to 4 pixels, along with a high-density pattern [32]. It is recommended to assess the speckle size prior to conducting the test. Furthermore, employing a camera with higher resolution becomes necessary to accurately detect smaller patterns.

The findings for Type III are presented in Figure 8. The stress-strain curve for Exx, the stress-strain curve for Eyy, and the average strain curve for Exx and Eyy exhibit patterns akin to those observed in Type I and Type II results. Notably, the R2 values of Figure 8 (a) and (b) are higher than 0.95, indicating minimal disturbances and smooth alignment. These behaviors can be attributed to the specimen's geometry, as Type III specimens have the largest area along the gauge length, facilitating the presence of abundant speckle patterns that can be easily detected by a smartphone camera and analyzed using the Ncorr code. Consequently, Type III specimens yield the clearest and smoothest data points in the analysis.

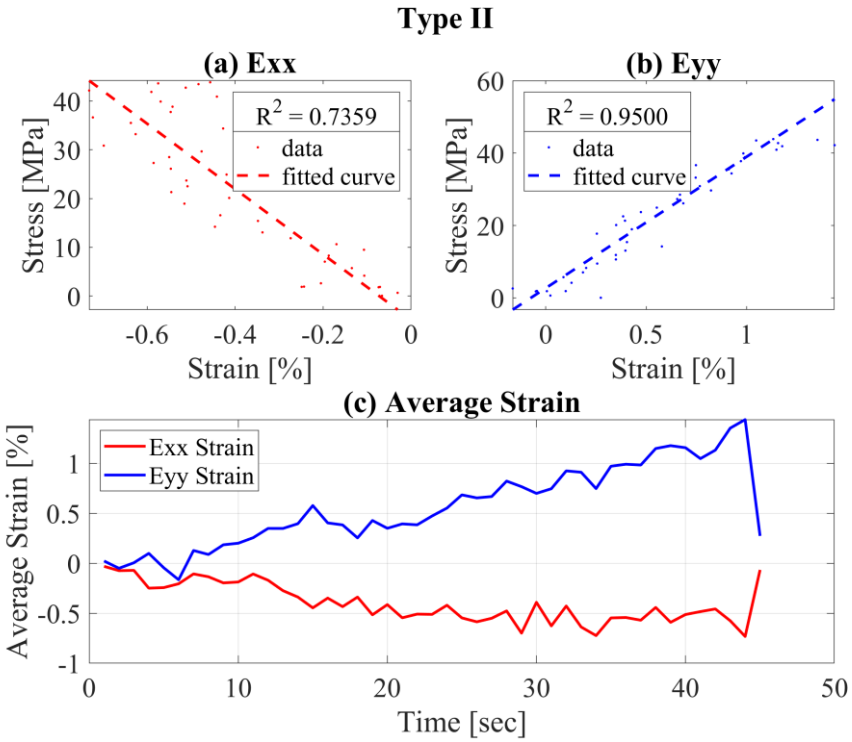

Figure 7. Type II Results

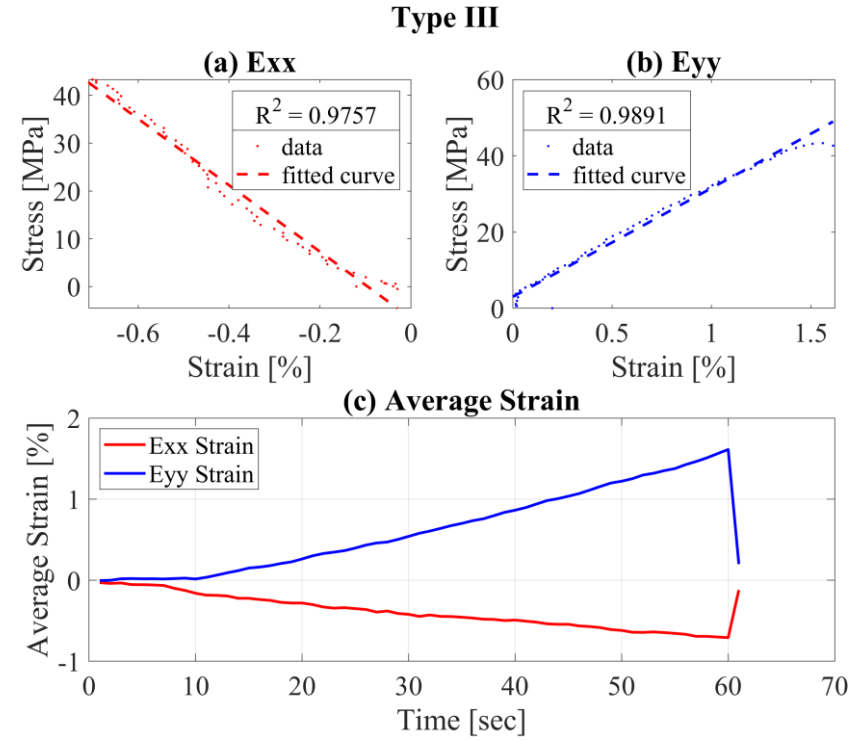

Figure 8. Type III Results

Figure 9 and Figure 10 present the outcomes for Type IV and Type V, respectively. The stress-strain curves for Exx, Eyy, and the average strain curves for Exx and Eyy exhibit similarities to the results observed in previous types. However, it is notable that the data points are relatively fewer in Types IV and V. This can be attributed to the shorter duration until a fracture occurs, leading to a reduced number of frames captured during the experiment.

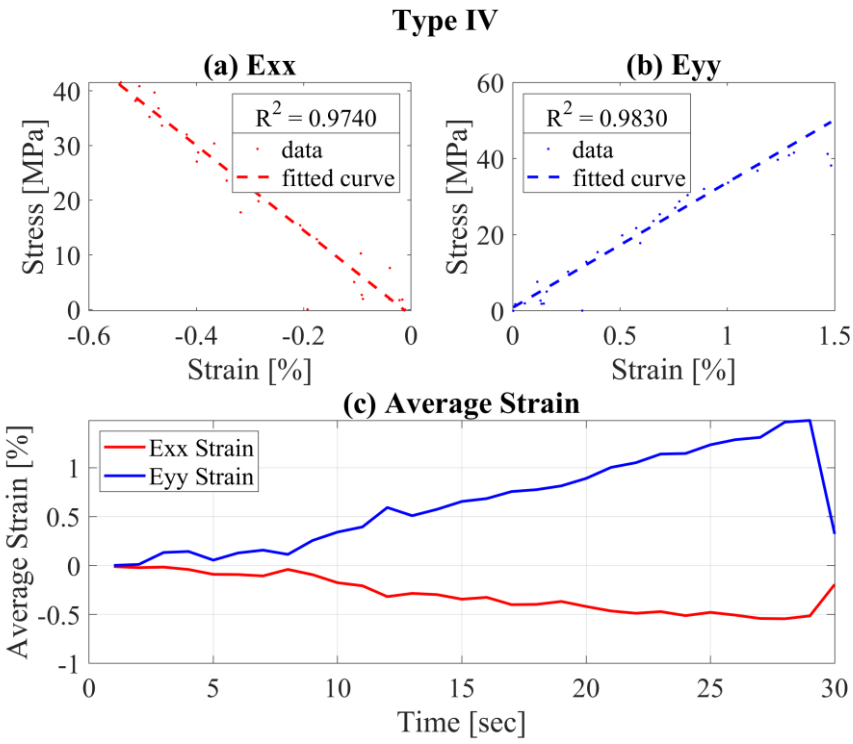

Figure 9. Type IV Results

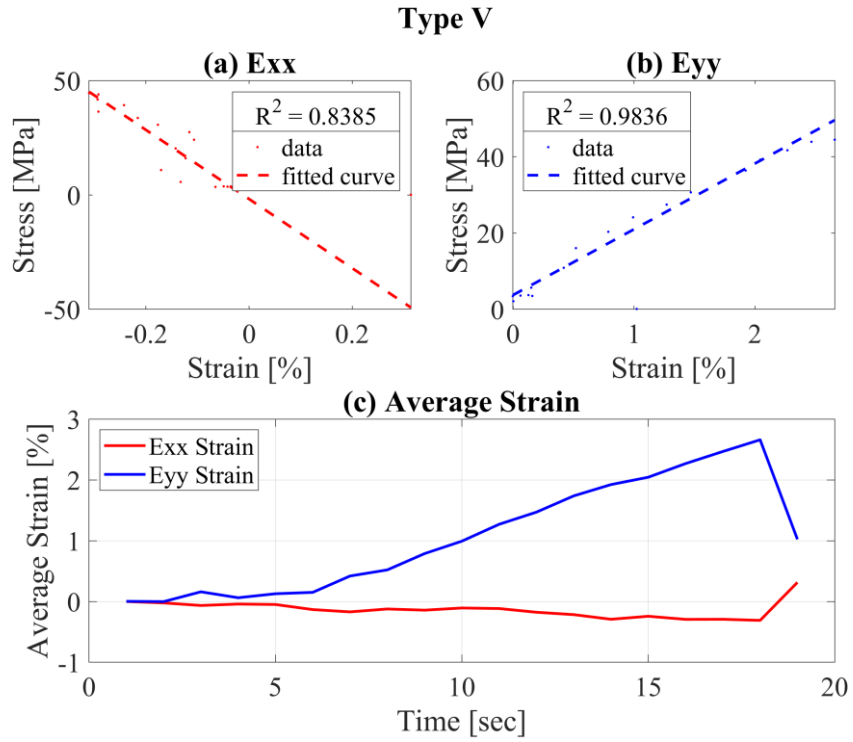

Figure 10. Type V Results

In Figures 6 to 10, the majority of R^2 values are above 0.9, illustrating a strong correlation between the experimental data and the fitted curves, improving the reliability and clarity of the results used for comparison. Moreover, the average strain by time graphs provide insight into the behavior of strains along the x- and y-axes simultaneously. Eyy shows an increasing trend over time, while Exx exhibits a decreasing trend. This dynamic is a consequence of the specimen elongating along the y-axis under applied tensile load while simultaneously contracting along the x-axis, leading to necking in the specimen. The smoothness of these curves relies heavily

on precise displacement measurements facilitated by the DIC method. Similar to the challenges encountered with noise in Type II results, any noise or spike behavior observed in the Exx and Eyy graphs against time can be attributed to factors such as the speckle pattern size and the resolution of the camera used for measurement.

Figure 11 presents the average UTS for each ASTM-D638 type in ascending order. The maximum stress of each specimen is carefully recorded, considering the different specimen types. It is determined that Type IV exhibited the weakest performance, with a UTS of 40.302 MPa. Following closely is Type V, with a UTS of 42.640 MPa, having the highest standard deviation. Type III demonstrated a UTS of 43.019 MPa, along with the lowest standard deviation. Comparatively, Type II and Type I display the highest UTS values, measuring 43.164 MPa and 43.179 MPa, respectively, with a marginal difference of 0.015 MPa between them. Consequently, it can be inferred that Type I is the most suitable choice among the ASTM-D638 specimen types for conducting tests to ascertain the tensile properties of PLA 3D-printed specimens.

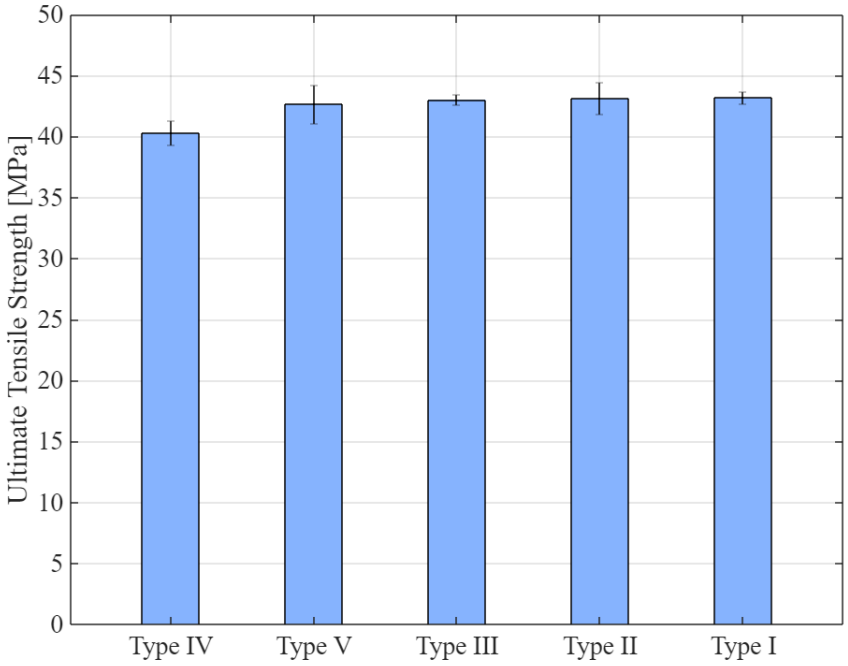

Figure 11. Average Ultimate Tensile Strength of each ASTM-D638 Type

The current study results for UTS values fall within the range of values reported earlier in the literature on FDM-printed PLA parts tested under the ASTM D638 standard. For example, Jatti et al. [15] found a UTS of 55.475 MPa using a Type V specimen under optimal print conditions. Whereas Syaefudin et al. [16] reported a UTS of 35.16 MPa for Type IV specimens. Yeole [18] also utilized Type IV specimens and obtained a higher UTS of 54.46 MPa. This variation of UTS values for the same specimen type (Type IV) can be attributed to the varying print settings tailored for maximum strength. Letcher and Waytashek [17] reported a UTS of approximately 58 MPa for Type I specimens, despite some dimensional deviations. These comparative values support the current study and strengthen the influence of specimen type and process parameters on the tensile characteristics of FDM printed PLA parts. It also supports the reliability of the DIC-based tensile testing technique and the defined printing parameters utilized.

Several reasons could be the cause of the variation between the UTS values found in the current study and the literature. Prior research used different printing parameters designed for maximal strength (e.g., higher extrusion temperature or lower layer thickness), while the current study maintained a set of defined and uniform parameters for all specimen types Table 2 . The printing parameters were established based on the literature data, along with a trial-and-error methodology to fulfill the geometric requirements of all ASTM-D638 specimen types without

negatively influencing the strength properties of the part. Therefore, by defining the printing parameters, the current study focused on merely identifying the impact of specimen geometry. In addition, the difference in reported results is also due to the difference in the test equipment being utilized (i.e., utilization of DIC or extensometers), the surrounding environment, printer models, tensile testing machines, and filament manufacturers.

Table 4. 3D-Printing Data Per Specimen

Samples Type	***Printing Time (hours, minutes, seconds)***	***Filament Usage (gram, meter)***
Type I	1 hr, 18 min, 31 sec	9.8 g/3.30 m
Type II	1 hr, 9 min, 45 sec	8.3 g/2.80 m
Type III	3 hr, 5 min, 27 sec	23 g/7.70 m
Type IV	48 min, 38 sec	5.7 g/1.91 m
Type V	14 min, 59 sec	1.8 g/0.60 m

One important aspect to be considered during this research is assessing the efficiency of 3D-printing for the five sample types. The optimization of 3D-printing processes should not only consider the mechanical properties, such as the UTS of the printed parts, but also consider balancing between factors such as printing time, filament usage, and cost-effectiveness. The two factors, printing time and filament usage, are shown in Table 4, where the data for those two factors is obtained from the slicer software ideaMaker. Printing Time: represents how long it takes to print a specimen of each type. Filament Usage: represents how much filament (in grams and meters) is consumed during the printing process. The cost-effectiveness encompasses not only the direct expenses associated with filament usage but also broader economic factors such as equipment maintenance and wear resulting from prolonged machine usage, which includes the 3D-printer and the tensile testing machine in the scope of this research. Maintenance requirements, such as replacing the 3D-printer cooler fan, were required in conducting this study.

Based on the recorded data, some deductions about the 3D-printing process efficiency can be drawn. Type V is the fastest to print, taking only 14 minutes and 59 seconds. Type IV is the second fastest, followed by Type II, and then Type I. Type III takes significantly longer than the other types, requiring 3 hours, 5 minutes, and 27 seconds. Similarly, Type V consumes the least amount of filament, followed by Type IV. Type II has moderate filament usage, while Type I uses a relatively higher amount compared to Type II. Type III uses the highest amount of filament. Therefore, it can be estimated that the printing time for Type V took approximately 5 times less than Type I.

In summary, along with the mechanical properties, considering printing time, filament usage, and cost-effectiveness of the 3D-printing the overall printing efficiency of these sample types, Type V shows to be the most efficient choice for 3D-printing in terms of balancing between mechanical efficiency and printing efficiency while Type IV, Types I, and II are somewhat less efficient due to longer printing times and moderate filament usage. On the other hand, Type III is the least efficient option because it has the longest printing time and the highest filament usage.

Therefore, taking into consideration the 3D-printing process efficiency along with the tensile properties, while Type I was found to have the highest UTS value of 43.179 MPa, it cannot be deduced to be the most efficient specimen type due to its drastically high consumption of filament as well as long printing time. This high UTS comes at a cost of approximately 5 times longer print time and more than 5 times the filament amount than type V. Moreover, Type V was proven to exhibit a reasonable UTS value of 42.640 MPa with a negligible difference of 0.539 MPa compared to Type I. Therefore, it can be concluded that Type V is the most efficient ASTM-D638 specimen type due to its low filament usage and printing time during the production process and acceptable mechanical properties.

4. Discussion and Conclusion

In conclusion, this research aimed to investigate the influence of ASTM-D638 specimen type on the mechanical properties of 3D-printed PLA materials. The study employed an FDM 3D-printing technique to produce PLA specimens, followed by tensile testing and DIC analysis for deformation measurement. The research addressed a gap in the literature regarding the impact of specimen design on the mechanical properties of 3D-printed parts and provided valuable insights for future studies. The experimental methodology involved CAD modeling, printing parameter optimization, surface preparation, DIC setup, and tensile testing using a Shimadzu machine. MATLAB was used for data analysis, resulting in stress-strain curves and UTS values for each specimen type.

Determining the best specimen type depends on the factors of filament usage, printing time, and cost efficiency, as well as the average UTS for each ASTM-D638 type. In terms of production efficiency, Type V is found to be the most efficient display, as it consumes the lowest filament, the shortest printing time, and consequently is the most cost-efficient due to its geometrical dimensions. Whereas, in terms of strength, Type I exhibits the highest UTS value; however, Type V showed an acceptable UTS value with a marginal difference of 0.539 MPa less than Type I.

Therefore, considering the factors of production efficiency and strength, it appears that Type V is the best option. It has a short printing time, low filament usage, and a reasonable value of UTS of 42.640 MPa, making it a suitable choice among the ASTM-D638 specimen types for conducting further research on 3D-printed PLA specimens. However, it is important to note that the most efficient ASTM-D63 specimen type, between Type I and Type V, can vary depending on the application case, such as rapid prototyping or certification testing.

ACKNOWLEDGMENT

The successful completion of this project was made possible through the funding provided by TÜBİTAK, the Scientific and Technological Research Institution of Turkey, under the grant TÜBİTAK–2209-A University Students Research Projects Support Program. Their support was instrumental in advancing our research endeavors and achieving our project goals.

REFERENCES

[1] Wickramasinghe S, Do T, Tran P. FDM-based 3D printing of polymer and associated composite: A review on mechanical properties, defects and treatments. Polymers (Basel) 2020;12:1529.

[2] Berman B. 3-D printing: The new industrial revolution. Bus Horiz 2012;55:155–62.

[3] Shanmugam R, Ramoni MO, Chandran J, Mohanavel V, Pugazhendhi L. A Review on the significant classification of Additive Manufacturing. J Phys Conf Ser, vol. 2027, IOP Publishing; 2021, p. 012026.

[4] Cano-Vicent A, Tambuwala MM, Hassan SS, Barh D, Aljabali AAA, Birkett M, et al. Fused deposition modelling: Current status, methodology, applications and future prospects. Addit Manuf 2021;47:102378.

[5] Mushtaq RT, Iqbal A, Wang Y, Rehman M, Petra MI. Investigation and Optimization of Effects of 3D Printer Process Parameters on Performance Parameters. Materials 2023;16:3392.

[6] Penumakala PK, Santo J, Thomas A. A critical review on the fused deposition modeling of thermoplastic polymer composites. Compos B Eng 2020;201:108336.

[7] Ćwikła G, Grabowik C, Kalinowski K, Paprocka I, Ociepka P. The influence of printing parameters on selected mechanical properties of FDM/FFF 3D-printed parts. IOP Conf Ser Mater Sci Eng, vol. 227, IOP Publishing; 2017, p. 012033.

[8] Tymrak BM, Kreiger M, Pearce JM. Mechanical properties of components fabricated with open-source 3-D printers under realistic environmental conditions. Mater Des 2014;58:242–6.

[9] Ansari AA, Kamil M. Effect of print speed and extrusion temperature on properties of 3D printed PLA using fused deposition modeling process. Mater Today Proc 2021;45:5462–8.

[10] Singh R, Singh J, Singh S. Investigation for dimensional accuracy of AMC prepared by FDM assisted investment casting using nylon-6 waste based reinforced filament. Measurement 2016;78:253–9.

[11] Popescu D, Zapciu A, Amza C, Baciu F, Marinescu R. FDM process parameters influence over the mechanical properties of polymer specimens: A review. Polym Test 2018;69:157–66.

[12] Kamaal M, Anas M, Rastogi H, Bhardwaj N, Rahaman A. Effect of FDM process parameters on mechanical properties of 3D-printed carbon fibre–PLA composite. Progress in Additive Manufacturing 2021;6:63–9.

[13] Kam M, Ipekci A, Şengül Ö. Investigation of the effect of FDM process parameters on mechanical properties of 3D printed PA12 samples using Taguchi method. Journal of Thermoplastic Composite Materials 2023;36:307–25.

[14] Qattawi A, Alrawi B, Guzman A. Experimental optimization of fused deposition modelling processing parameters: a design-for-manufacturing approach. Procedia Manuf 2017;10:791–803.

[15] Jatti VS, Tamboli S, Shaikh S, Solke NS, Gulia V, Jatti VS, et al. Optimization of tensile strength in 3D printed PLA parts via meta-heuristic approaches: a comparative study. Front Mater 2024;Volume 10-2023.

[16] Syaefudin E, Kholil A, Hakim M, Wulandari D, Riyadi R, Murtinugraha E. The effect of orientation on tensile strength 3D printing with ABS and PLA materials. J Phys Conf Ser 2023;2596:012002. https://doi.org/10.1088/1742-6596/2596/1/012002.

[17] Letcher T, Waytashek M. Material Property Testing of 3D-Printed Specimen in PLA on an Entry-Level 3D Printer. vol. 2. 2014. https://doi.org/10.1115/IMECE2014-39379.

[18] Yeole SN. Tensile Testing and Evaluation of 3D Printed PLA Specimens as per ASTM D638 Type-IV Standard. 2018.

[19] McCormick N, Lord J. Digital image correlation. Materials Today 2010;13:52–4.

[20] Khoo S-W, Karuppanan S, Tan C-S. A review of surface deformation and strain measurement using two-dimensional digital image correlation. Metrology and Measurement Systems 2016;23:461–80.

[21] Peters WH, Ranson WF. Digital imaging techniques in experimental stress analysis. Optical Engineering 1982;21:427–31.

[22] Wang CCB, Deng J-M, Ateshian GA, Hung CT. An automated approach for direct measurement of two-dimensional strain distributions within articular cartilage under unconfined compression. J Biomech Eng 2002;124:557–67.

[23] Lecompte D, Smits A, Bossuyt S, Sol H, Vantomme J, Van Hemelrijck D, et al. Quality assessment of speckle patterns for digital image correlation. Opt Lasers Eng 2006;44:1132–45.

[24] Crammond G, Boyd SW, Dulieu-Barton JM. Speckle pattern quality assessment for digital image correlation. Opt Lasers Eng 2013;51:1368–78.

[25] Yaofeng S, Pang JHL. Study of optimal subset size in digital image correlation of speckle pattern images. Opt Lasers Eng 2007;45:967–74.

[26] Berfield TA, Patel JK, Shimmin RG, Braun P V, Lambros J, Sottos NR. Micro-and nanoscale deformation measurement of surface and internal planes via digital image correlation. Exp Mech 2007;47:51–62.

[27] Pan B, Li K. A fast digital image correlation method for deformation measurement. Opt Lasers Eng 2011;49:841–7.

[28] Blaber J, Adair B, Antoniou A. Ncorr: open-source 2D digital image correlation matlab software. Exp Mech 2015;55:1105–22.

[29] Ali MB, Ab Ghani AF, DharMalingam S, Mahmud J. Digital image correlation (DIC) technique in measuring strain using opensource platform Ncorr. Journal of Advanced Research in Applied Mechanics 2016;26:10–21.

[30] Altahir S, Gomaa R, Yilmaz C. Effect of strain rate on the tensile properties of 3D–printed PLA specimens with fused deposition modelling. Journal of Advances in Manufacturing Engineering 2024;5:37–46.

[31] PLA+ n.d. https://www.esun3d.com/pla-pro-product/ (accessed August 21, 2024).

[32] Hua T, Xie H, Wang S, Hu Z, Chen P, Zhang Q. Evaluation of the quality of a speckle pattern in the digital image correlation method by mean subset fluctuation. Opt Laser Technol 2011;43:9–13. https://doi.org/https://doi.org/10.1016/j.optlastec.2010.04.010.